

Supporting Information

Anion-Dependent Structural Variations and Charge Transport Property

Analysis of 4'-(3-pyridyl)-4,2':6',4''-terpyridinium Salts

Anowar Hossain,^a Arka Dey,^b Saikat Kumar Seth,^b Partha Pratim Ray,^b Joaquín Ortega-Castro,^c

Antonio Frontera*^c and Subrata Mukhopadhyay*^a

^aDepartment of Chemistry, Jadavpur University, Kolkata 700032, India

^bDepartment of Physics, Jadavpur University, Kolkata 700032, India

^cDepartament de Química, Universitat de les Illes Balears, Crta. de Valldemossa km 7.5, 07122

Palma de Mallorca, Balears, Spain

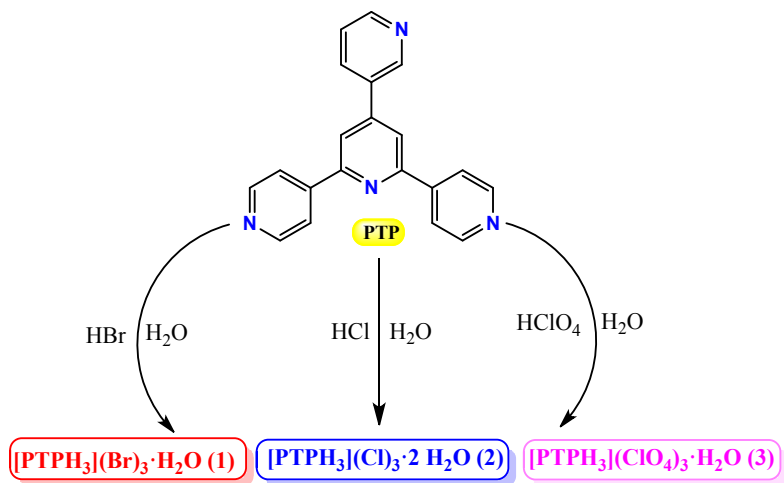
Computational details

The 2/m primitive monoclinic crystal (**1** and **2**) and $P\bar{1}$ primitive triclinic crystal (**3**) structures were optimized with the density functional theory method using the CASTEP program code of Accelrys, Inc.¹ It was relaxed with the experimental unit cell parameters fixed. The calculations were performed within the Generalized-Gradient approximation (GGA) and the Perdew-Burke-Ernzerhof (PBE) formulation for the exchange-correlation functional.^{2,3} Ultrasoft pseudopotentials⁴ were used in the geometric optimization of this work with the relativistic treatment of the Koelling-Harmon.⁵ A plane-wave basis set with 500 eV cutoff was applied. The k-mesh points over the Brillouin zone was generated with parameters 3×3×1 the Monkhorst-Pack-scheme for the monoclinic crystals and 2×1×1 for the triclinic crystal. The energy tolerance for self-consistent field (SCF) convergence was 2×10^{-6} eV/atom for all calculations. The long-range dispersion correction has been included in the calculations with the Tkatchenko-Scheffler scheme.⁶ Norm-conserving pseudopotentials with a cutoff the 600 eV were used for the property's calculations. Band structures were calculated along the k-vector of the first Brillouin zone of the crystal, and Total and Partial density of states (TDOS and PDOS, respectively) were plotted concerning the Fermi level with a 3×2×2 grid. The optical properties including dielectric function and optical conductivity of the crystal are calculated. Optical properties are calculated for plane polarized light with the specified polarization directions: (100) (010) (001). The smearing of 0.2 eV was employed.

For the analysis of noncovalent interactions, the energies of the complexes and assemblies were computed using Gaussian-16 program⁷ at the PBE0-D3/def2-TZVP level of theory. The anion- π interaction energies were computed by calculating the difference between the energies of the isolated monomers and the one of their assembly. The Grimme's D3 dispersion correction has

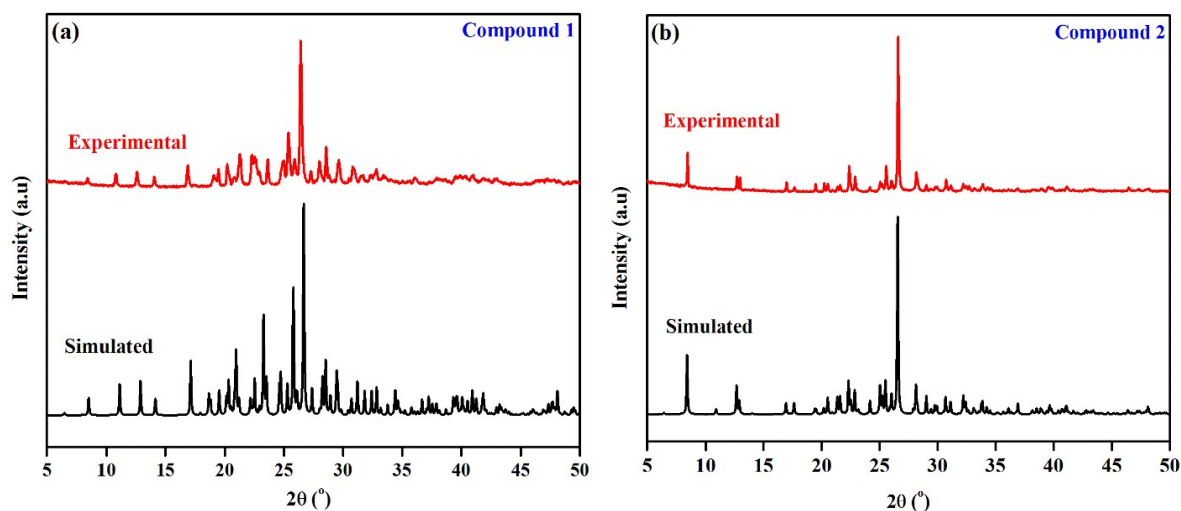
been used in the calculations.⁸ The QTAIM analysis⁹ and NCIPLOT index¹⁰ calculations have been computed at the same level of theory by means of the AIMAll program.¹¹

Scheme S1:



Scheme S1. Schematic representation for the synthesis of the compounds.

Figure S1:



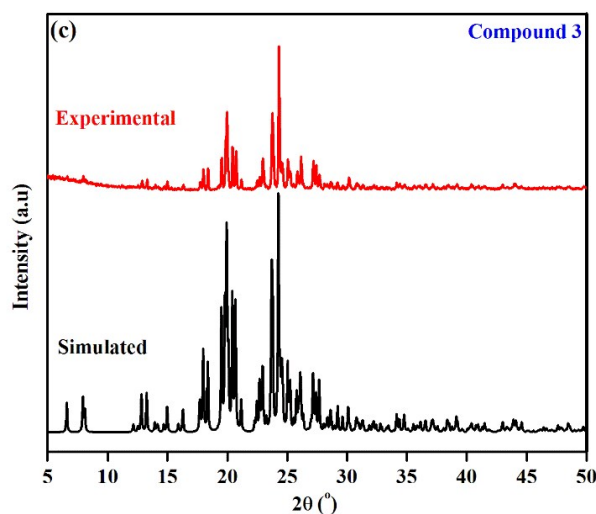


Fig. S1 PXRD patterns of all the three compounds **1**, **2** and **3**.

Structural description of compound **1**

Compound **1** crystallizes in monoclinic crystal system with ‘Cc’ space group (Table 1). In the asymmetric unit a triply protonated PTPH₃ unit, three bromide anion and a solvent water molecule are present (Fig. 1(a)). The solid state structure of **1** was stabilized by $\pi \cdots \pi^+$, N–H \cdots O, N–H \cdots Br, O–H \cdots Br, C–H \cdots O and C–H \cdots Br interactions. Geometrical parameters for different type of interactions are given in Tables S1 and S2.

Table S1 Relevant hydrogen bonding parameters (Å,°) for compounds **1–3**

Compound	D–H \cdots A	D–H	H \cdots A	D \cdots A	D–H \cdots A	Symmetry
1	O1–H1A \cdots Br2	0.84(9)	2.60(15)	3.353(11)	150(15)	1+x, y, z
	O1–H1B \cdots Br2	0.83(13)	2.40(14)	3.221(11)	173(17)	.
	N2–H2A \cdots Br1	0.86	2.61	3.326(8)	142	-3/2+x, 3/2-y, 1/2+z
	N3–H3A \cdots Br3	0.86	2.46	3.206(8)	146	1+x, y, z
	N4–H4A \cdots Br1	0.86	2.4	3.219(8)	160	.
	C2–H2 \cdots Br3	0.93	2.76	3.643(12)	159	-1/2+x, 3/2-y, 1/2+z
	C3–H3 \cdots O1	0.93	2.29	3.169(14)	158	-1+x, y, z
	C5–H5 \cdots Br2	0.93	2.67	3.572(9)	163	1/2+x, 3/2-y, -1/2+z
	C13–H13 \cdots Br2	0.93	2.83	3.594(8)	140	-1+x, y, z
C14–H14 \cdots Br3	0.93	2.85	3.474(9)	126	-1+x, 1-y, 1/2+z	
2	O1–H1A \cdots Cl2	0.85(5)	2.34(5)	3.187(4)	172(5)	-1+x, y, z

	O1–H1B···C12	0.84(5)	2.30(5)	3.121(4)	165(5)	.
	N2–H2A···C11	0.86	2.47	3.175(3)	140	3/2+x, 1/2-y, -1/2+z
	O2–H2C···C13	0.86(7)	2.23(6)	3.084(3)	171(11)	.
	O2–H2D···C11	0.85(9)	2.37(8)	3.087(4)	142(11)	1/2+x, 1/2-y, 1/2+z
	N3–H3A···C13	0.86	2.21	3.008(3)	155	-1+x, y, z
	N4–H4A···C11	0.86	2.22	3.044(3)	162	.
	C2–H2···C13	0.93	2.69	3.582(5)	161	1/2+x, 1/2-y, -1/2+z
	C3–H3···O1	0.93	2.33	3.235(5)	163	1+x, y, z
	C5–H5···C12	0.93	2.57	3.462(4)	161	-1/2+x, 1/2-y, 1/2+z
	C10–H10···C12	0.93	2.8	3.725(3)	174	-1/2+x, 1/2-y, 1/2+z
	C13–H13···C12	0.93	2.71	3.469(3)	140	1+x, y, z
	C14–H14···C13	0.93	2.81	3.424(4)	125	1+x, 1-y, -1/2+z
	C15–H15···O2	0.93	2.43	3.305(6)	156	x, 1-y, -1/2+z
	C17–H17···C12	0.93	2.64	3.560(3)	170	-1/2+x, 1/2-y, 1/2+z
	C20–H20···O2	0.93	2.29	3.144(6)	153	x, 1-y, -1/2+z
3	N2–H2A···O4	0.86	2.05	2.886(5)	164	x, 1+y, z
	N2–H2A···O9	0.86	2.60	2.915(7)	103	1+x, y, z
	N3–H3A···O1	0.86	1.83	2.681(6)	172	-1+x, y, z
	N4–H4A···O12	0.86	2.11	2.921(9)	158	x, -1+y, -1+z
	C15–H15···N1	0.93	2.44	2.758(5)	100	-
	C13–	0.93	2.59	3.290(9)	132	x, y, -1+z
	C7–H7···O10	0.93	2.48	3.197(9)	134	1-x, 1-y, 1-z
	C10–H10···O2	0.93	2.60	3.181(5)	121	-1+x, y, z
	C10–H10···O7	0.93	2.45	3.278(7)	149	x, -1+y, z
	C1–H1···O2	0.93	2.49	3.330(6)	151	1-x, -y, -z
	C5–H5···O5	0.93	2.55	3.121(6)	120	-
	C5–H5···O7	0.93	2.42	3.257(7)	149	x, -1+y, z
	C7–H7···O10	0.93	2.48	3.197(9)	134	1-x, 1-y, 1-z
	C17–H17···O2	0.93	2.57	3.269(6)	133	-1+x, y, z
	C17–H17···O7	0.93	2.58	3.330(7)	138	x, -1+y, z
	C18–H18···O8	0.93	2.40	3.302(8)	163	-x, 1-y, 1-z
	C20–H20···N1	0.93	2.43	2.761(5)	101	-
	C20–H20···O5	0.93	2.49	3.317(6)	149	1-x, 1-y, 1-z

Table S2 Geometrical parameters (Å, °) for the π -stacking moieties involved in the $\pi^+ \cdots \pi$ and $\pi^+ \cdots \pi^+$ interactions for the title compounds

Com	Cg(i)···Cg(j)	Cg(i)···Cg(j)	α (°)	β (°)	γ (°)	Cg(i)–	Cg(j)–	Symmetry
-----	---------------	---------------	--------------	-------------	--------------	--------	--------	----------

pound) [Å]				perp	perp [Å]	
						[Å]		
1	Cg(1)···Cg(2)	3.908(5)	7.40	34.16	26.82	3.488	3.234	1+x, y, z
	Cg(2)···Cg(1)	3.908(5)	7.40	26.82	34.16	3.234	3.488	-1+x, y, z
2	Cg(1)···Cg(2)	3.977(17)	6.22	36.21	30.00	3.445	3.210	-1+x, y, z
	Cg(2)···Cg(1)	3.978(17)	6.22	30.00	36.21	3.210	3.445	1+x, y, z
3	Cg(2)···Cg(3)	3.877(3)	10.85	24.54	14.40	3.755	3.526	1-x, 1-y, 1-z
	Cg(3)···Cg(2)	3.877(3)	10.85	14.40	24.54	3.527	3.755	1-x, 1-y, 1-z
	Cg(4)···Cg(4)	3.859(3)	0.00	22.34	22.34	3.569	3.569	-x, -y, -z

Cg(i) and Cg(j) denotes centroid of i-th and j-th ring respectively. For all the compounds Cg(1), Cg(2), Cg(3), and Cg(4) are the centroids of [N(1)/C(8)/C(7)/C(6)/C(10)/C(9)], [N(2)/C(13)/C(12)/C(11)/C(15)/C(14)], [N(3)/C(18)/C(17)/C(16)/C(20)/C(19)] and [N(4)/C(1)/C(2)/C(3)/C(4)/C(5)] rings respectively.

The bromide anion Br1 acts as acceptor for N2 and N4 in the molecule at (-3/2+x, 3/2-y, 1/2+z) and (x, y, z) respectively, whereas bromide anion Br2 acts as acceptor for C5 and C13 in the molecule at (1/2+x, 3/2-y, -1/2+z) and (-1+x, y, z) respectively (Table S1). These four cumulatively lead to the formation of R₄²(10) ring motif (Fig. S2). On the other side, bromide anion Br3 acts as an acceptor for N3 and C2 in the molecule at (1+x, y, z) and (-1/2+x, 3/2-y, 1/2+z) respectively, Br2 acts as acceptor for O1 and C5 in the molecule at (x, y, z) and (1/2+x, 3/2-y, -1/2+z) respectively and O1 acts as acceptor for C3 in the molecule at (-1+x, y, z) (Table S1). All of these noncovalent interactions produces a R₅³(19) ring motif (Fig. S2). Another R₃²(13) synthon was generated when Br2 acts as acceptor towards O1 and C13 in the molecule at(x, y, z) and (-1+x, y, z) respectively and O1 acts as acceptor for C3 in the molecule at (-1+x, y, z) (Fig. S2). All the three ring motifs (i.e. R₄²(10), R₅³(19) and R₃²(13)) include the common

bromide anion Br2. Combine action of these three synthons generates a 1D chain in the (101) plane (Fig. S2). The largest $R_{10}^5(44)$ ring motif was produced when Br1 acts as acceptor for N2 and N3 and Br3 acts as acceptor for C2, C14 and N3 (Fig. S3). The 1D chain described in Fig. S1 thus interconnected by the motif $R_{10}^5(44)$ and generated a 2D layer in (101) plane (Fig. S4).

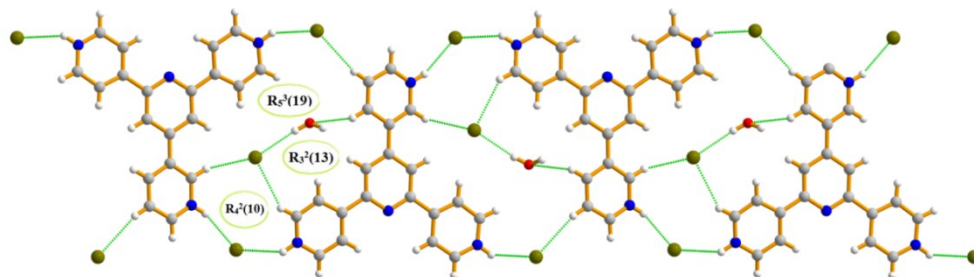


Fig. S2 Hydrogen bonded one dimensional chain in (101) plane in **1**.

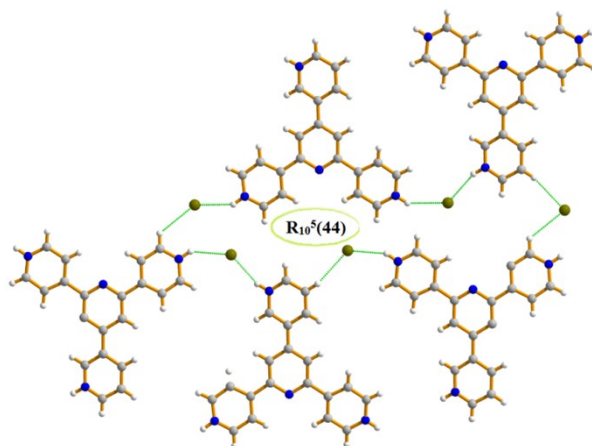


Fig. S3 Formation of $R_{10}^5(44)$ dimeric ring motif through C-H...Br and N-H...Br interactions in compound **1**.

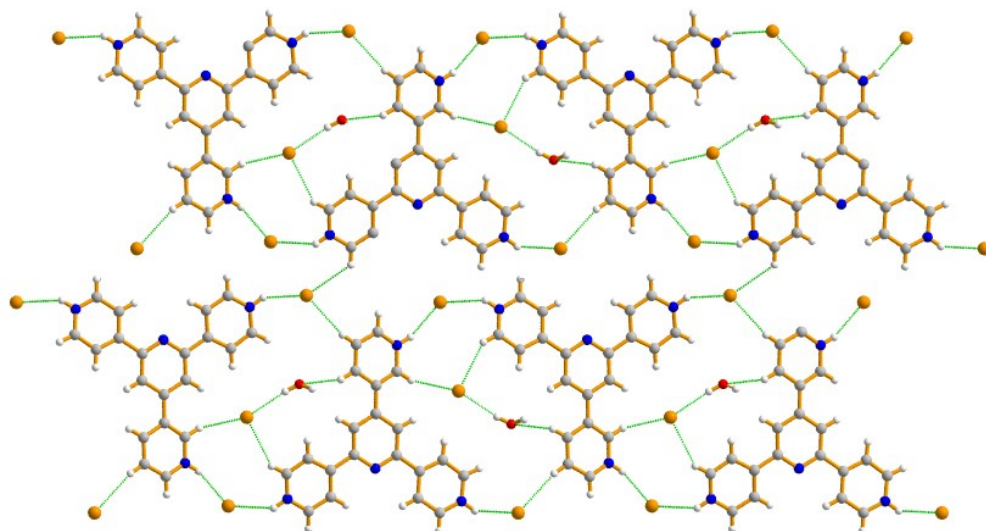


Fig. S4 2D layer in the (101) plane through O–H···Br, C–H···O, C–H···Br and N–H···Br interactions.

The bromide anion Br²⁻ by cooperative O–H···Br hydrogen bonding forms a one-dimensional water-bromide zigzag chain along [100] direction when acting as acceptor towards the only solvent water oxygen O1 in the molecule at (1+x, y, z) and (x, y, z) respectively (Fig. S5). In the water-bromide chain all the atoms are in the same plane bearing equal O···Br···O (87.14°) and Br···O···Br (95.67°) angles.

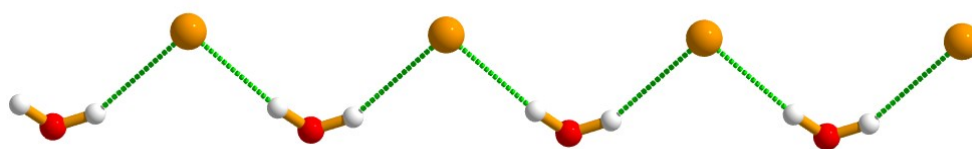


Fig. S5 One dimensional water-bromide zigzag chain along [100] direction in compound **1**.

Structural description of compound **2**

Compound **2** also crystallizes in monoclinic crystal system with ‘Cc’ space group (Table 1). Here, the asymmetric unit contains a triply protonated PTPH₃ unit along with three chloride anion and two solvent water molecules (Fig. 1(b)). For this compound stabilization was provided by $\pi\cdots\pi^+$, N–H···O, N–H···Cl, O–H···Cl, C–H···O and C–H···Cl interactions. Geometrical

parameters for different type of interactions are given in Tables S1 and S2. In the solid state, the chloride anion Cl1 acts as acceptor for N2 and N4 in the molecule at $(3/2+x, 1/2-y, -1/2+z)$ and (x, y, z) respectively, whereas chloride anion Cl2 acts as acceptor for C5 and C13 in the molecule at $(-1/2+x, 1/2-y, 1/2+z)$ and $(1+x, y, z)$ respectively (Table S1). These four cumulatively leads to the formation of $R_4^2(10)$ ring motif (Fig. S6). On the other side, chloride anion Cl3 acts as acceptor for N3 and C2 in the molecule at $(-1+x, y, z)$ and $(1/2+x, 1/2-y, -1/2+z)$ respectively, Cl2 act as acceptor for O1 and C17 in the molecule at (x, y, z) and $(-1/2+x, 1/2-y, 1/2+z)$ respectively and O1 acts as acceptor for C3 at $(1+x, y, z)$ (Table S1). All of these interactions generates a $R_5^3(13)$ ring motifs (Fig. S6). Another $R_3^2(13)$ synthon was generated when Cl2 acts as acceptor for O1 and C13 at (x, y, z) and $(1+x, y, z)$ respectively and O1 acts as acceptor for C3 at $(1+x, y, z)$ (Fig. S6). There are also two smallest synthons $R_2^1(7)$ present in the solid state. In one synthon, Cl2 acts as acceptor towards C5 and C10 at $(-1/2+x, 1/2-y, 1/2+z)$ (Table S1). Second smallest synthon was generated when chloride anion Cl2 acts as acceptor towards C10 and C17 at $(-1/2+x, 1/2-y, 1/2+z)$ (Table S1). All of the aforesaid ring motifs (i.e. $R_4^2(10)$, $R_5^3(13)$, $R_3^2(13)$ and two $R_2^1(7)$) are interconnected via common chloride anion Cl2. Repetition of these five ring motifs generates an infinite 1D chain in the (101) plane (Fig. S6). These 1D chains are further interconnected by O–H \cdots Cl (O2–H2C \cdots Cl3 and O2–H2D \cdots Cl1), N3–H3A \cdots Cl3 and C–H \cdots Cl (C14–H14 \cdots Cl3 and C2–H2 \cdots Cl3) interactions to generate $R_7^4(19)$, $R_6^4(16)$, $R_5^3(13)$ and $R_2^1(10)$ ring motifs (Fig. S7). These finally results in the formation of a 2D layer in (101) plane (Fig. S8).

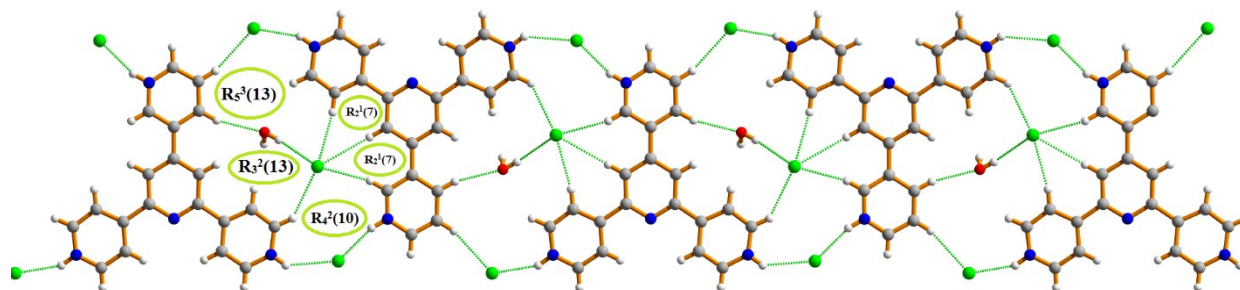


Fig. S6 Hydrogen bonded one dimensional chain in (101) plane in **2**.

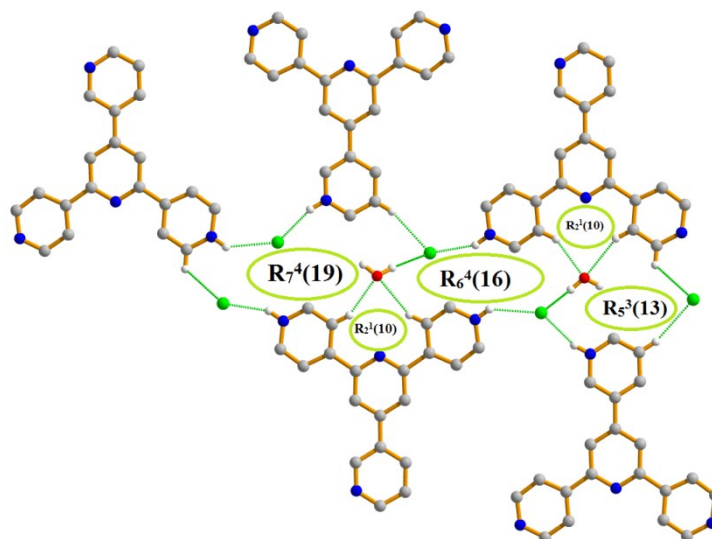


Fig. S7 Formation of $R_7^4(19)$, $R_6^4(16)$, $R_2^1(10)$ and $R_5^3(13)$ ring motifs through $O-H\cdots Cl$, $C-H\cdots O$, $C-H\cdots Cl$ and $N-H\cdots Cl$ interactions in compound **2**.

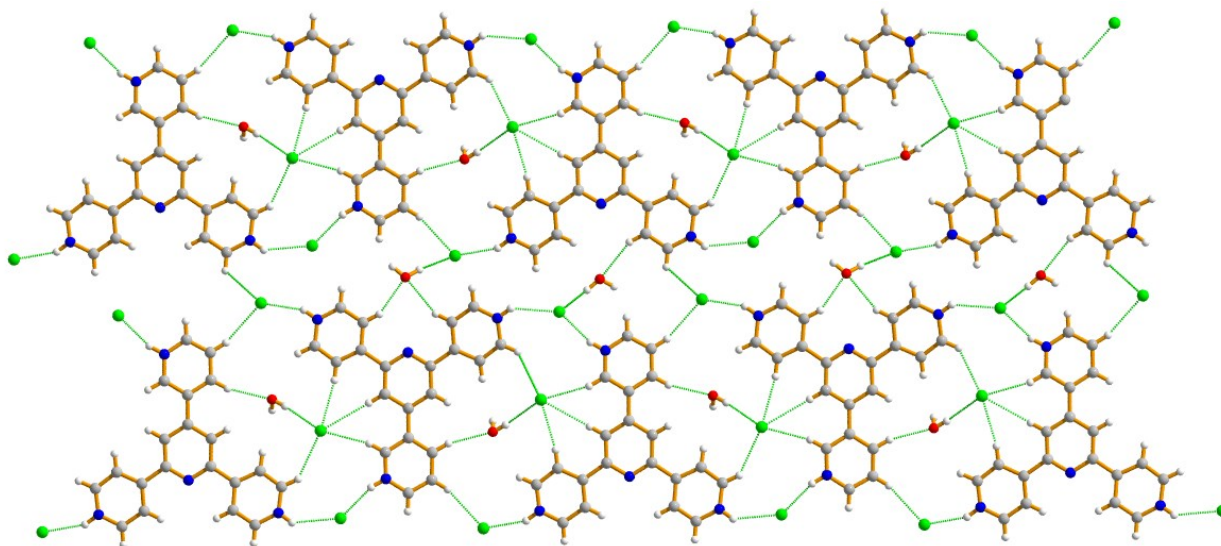


Fig. S8 2D layer in the (101) plane through O–H···Cl, C–H···O, C–H···Cl and N–H···Cl interactions.

Compound **2** also generates a one-dimensional water-chloride zigzag chain along [100] direction (Fig. S9). Here Cl1 acting as acceptor towards H1A and H1B of the solvent water oxygen O1 at (-1+x, y, z) and (x, y, z) respectively (Table S1). In the water-chloride chain all the atoms lie in the same plane and both the angles (O···Cl···O and Cl···O···Cl) are 95.94°.

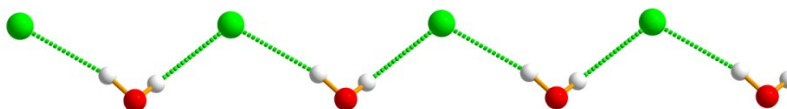


Fig. S9 One dimensional water-chloride zigzag chain along [100] direction in compound **2**.

Structural description of compound **3**

Compound **3** crystallizes in triclinic crystal system with ‘P-1’ space group (Table 1). Here, the asymmetric unit contains a triply protonated PTPH₃ unit, three perchlorate anion and a solvent water molecule (Fig. 1(c)). The solid state structure of compound **3** was stabilized by $\pi^+ \cdots \pi^+$, anion··· π^+ , anion··· π , N–H···O, C–H···N and C–H···O interactions. It has completely different solid state architecture from compounds **1** and **2**. In this compound, O7 and O8 act as acceptors for C17 and C18 in the molecule at (x, -1+y, z) and (-x, 1-y, 1-z) respectively (Table S1). These two C–H···O interactions generate $R_4^4(14)$ ring motifs (Fig. S10). On the other side, O10 and O12 act as acceptor for C7 and C13 in the molecule at (1-x, 1-y, 1-z) and (x, y, -1+z) respectively and generate a $R_4^4(20)$ ring motif (Fig. S10). Beside these large ring motifs two smallest $R_2^1(7)$ ring motifs were generated when O7 acts as an acceptor for ring carbon C5, C10 and C17 in the molecule at (x, -1+y, z) (Table S1). Sequential repetition of these ring motifs generates a 1D chain in (100) plane (Fig. S10). Two such 1D chains are further interconnected by $R_8^6(38)$ and $R_4^4(20)$ ring motifs (Fig. S11) and generate a 2D layer in the same (100) plane

(Fig. S12). Here, $R_8^6(38)$ ring motif was generated when O12 acts as acceptor for C13 and N4A at $(x, y, -1+z)$ and $(x, -1+y, -1+z)$ respectively, O7 acts as acceptor for C5 at $(x, -1+y, z)$ and O8 acts as acceptor for C18 at $(-x, 1-y, 1-z)$. The $R_4^4(20)$ ring motif was generated when O10 and O12 act as acceptor for C7 and N4A respectively in the molecule at $(1-x, 1-y, 1-z)$ and $(x, -1+y, -1+z)$ respectively (Table S1).

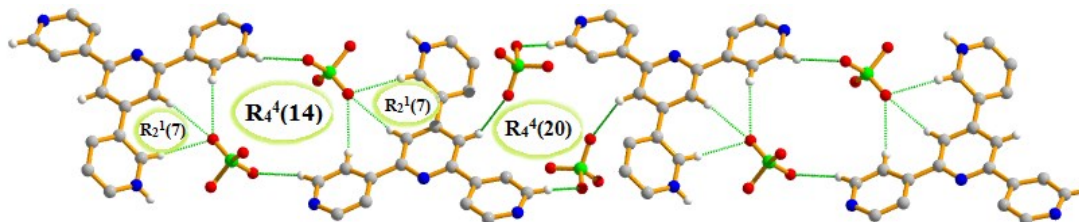


Fig. S10 Hydrogen bonded one dimensional chain in (100) plane in **3**.

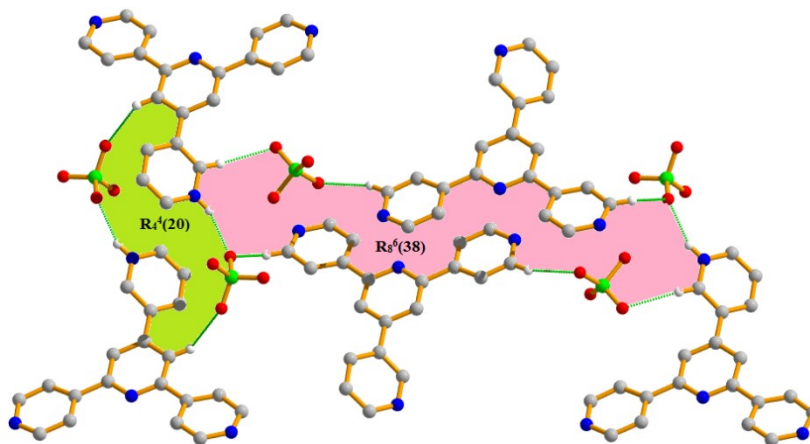


Fig. S11 Formation of $R_4^4(20)$ and $R_8^6(38)$ ring motifs through C–H \cdots O and N–H \cdots O hydrogen bonding interactions in **3**.

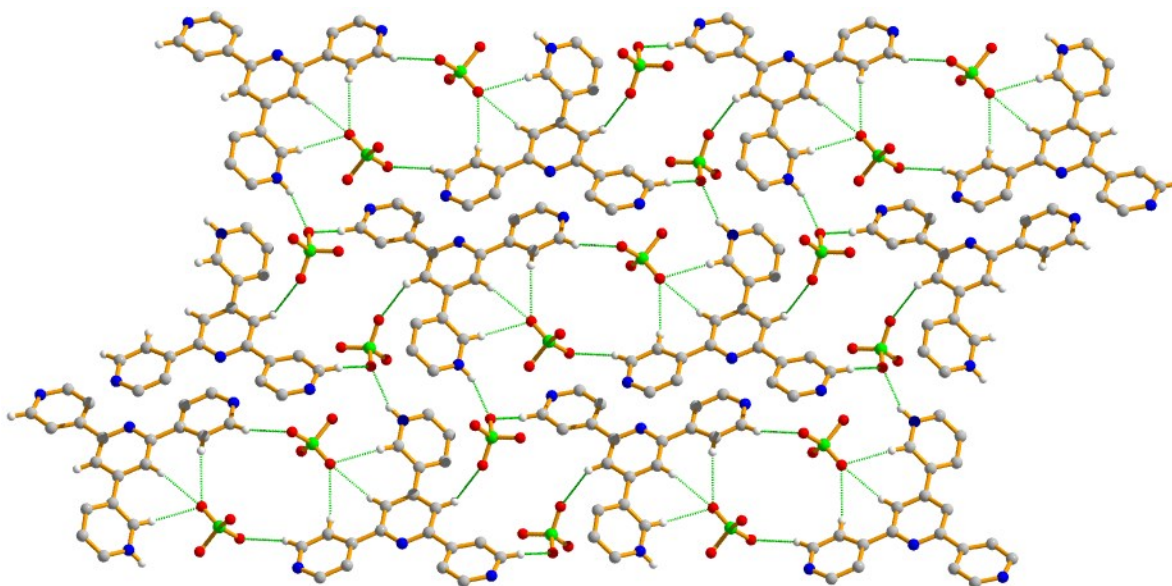


Fig. S12 2D layer in the (100) plane generated through C–H···O and N–H···O hydrogen bonding interactions.

Two different types of 2D layers, generated by different ClO_4^- anions, participated in the stabilization of the solid state structure of compound **3**. In one case, C11 containing ClO_4^- forms the 2D layer using anion··· π , N–H···O and C–H···O interactions (Fig. S13). Here, the anion··· π interaction is produced when O5 of perchlorate anion in the molecule at (x, y, z) is oriented toward the π -cloud of pyridine ring (A) in the molecule at (x, y, z), where the separation distance between the ring centroid and O5 atom [$\text{O5}\cdots\text{Cg}(1)$] is 3.384(4) Å. The shortest separation distance reflecting this interaction is $\text{O5}\cdots\text{C10} = 3.05$ Å, which is below the sum of the corresponding van der Waals radii (sum of van der Waals radii of O and C is 3.22 Å),⁷ thus suggesting significant anion··· π interaction. By using these novel anion··· π interaction along with weak $\text{C10-H10}\cdots\text{O2}$ and $\text{C17-H17}\cdots\text{O2}$ interactions lead to the formation of 1D chain along [100] direction. These 1D chains are further interconnected by strong $\text{N2-H2A}\cdots\text{O4}$ hydrogen bond at (x, 1+y, z) and propagates in a 2D layer in the (001) plane (Fig. S13).

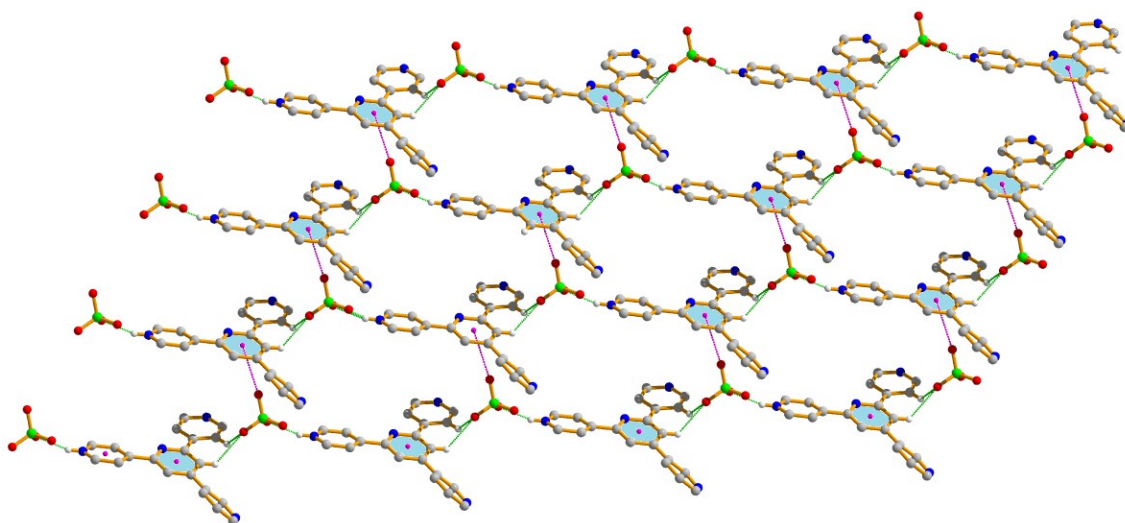


Fig. S13 2D layer in the (001) plane generated through anion $\cdots\pi$, C–H \cdots O and N–H \cdots O interactions.

The second 2D layer is formed using similar type interactions as mention above. The ClO_4^- anion participated in the formation of the 2D layer contain Cl2 atom. Here anion $\cdots\pi^+$ interaction instead of anion $\cdots\pi$ interaction strengthen the 2D layer. In this case, both O6 and O8 of perchlorate anion in the molecule at (x, y, z) are oriented toward the π -cloud of pyridinium ring (B) at (x, y, z) with a separation distance of $\text{O6}\cdots\text{Cg}(2) = 3.929(6) \text{ \AA}$ and $\text{O8}\cdots\text{Cg}(2) = 3.051(6) \text{ \AA}$. In this case the shortest separation distances are $\text{O6}\cdots\text{C13} = 3.473(3) \text{ \AA}$ and $\text{O8}\cdots\text{C14} = 3.101(2) \text{ \AA}$, whereas the sum of van der Waals radii of O and C is 3.22 \AA . Therefore, this represent the significant anion $\cdots\pi^+$ interactions. Combine action of these anion $\cdots\pi^+$ interactions along with the weak C–H \cdots O (C5–H5 \cdots O7, C10–H10 \cdots O7 and C17–H17 \cdots O7) interactions generates a 1D chain along [010] direction. These 1D chains are further interconnected by strong N2–H2A \cdots O9 hydrogen bond and generates a two-dimensional layer in (001) plane (Fig. S14).

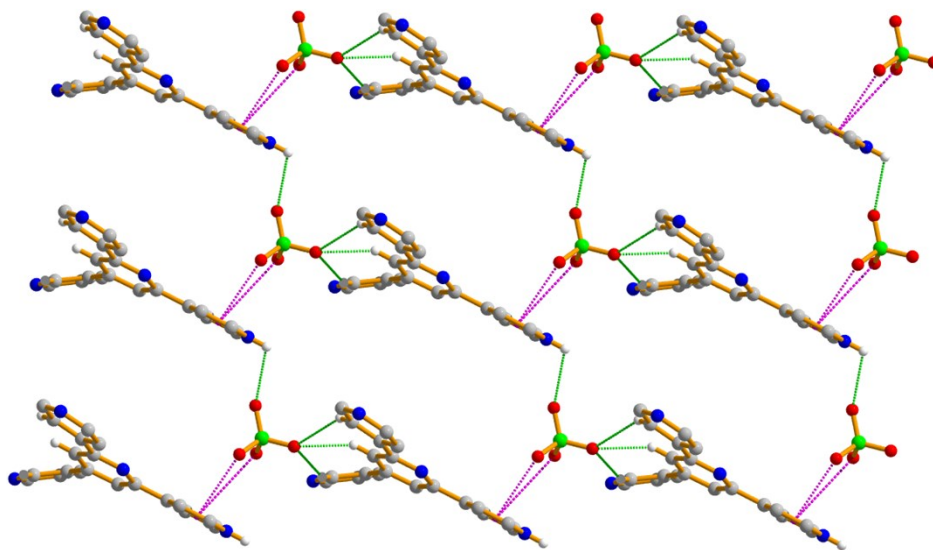


Fig. S14 2D layer in the (001) plane generated through anion $\cdots\pi^+$, N-H \cdots O and C-H \cdots O interactions.

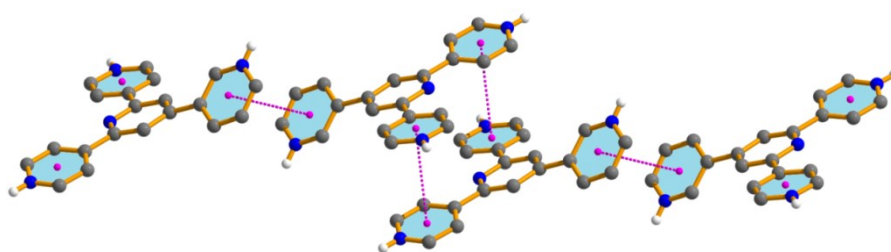


Fig. S15 $\pi^+\cdots\pi^+$ stacked 1D chain in compound **3**.

Optical characterization

The photophysical property of each compound (**1–3**) has been performed based on UV-vis spectrum. As the synthesized compounds produce stable dispersion in DMF, thin films on normal glass substrate were prepared for solid-state UV-vis spectroscopy.

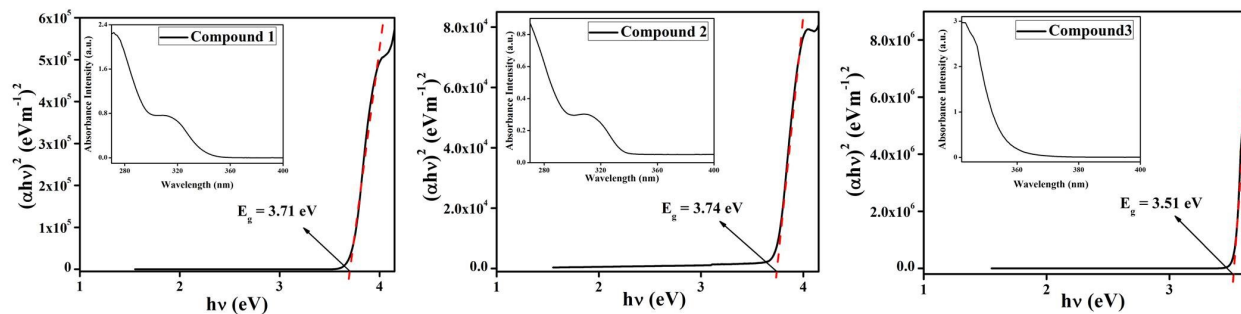


Fig. S16 UV-vis absorption spectra (inset) and Tauc's plots for compounds **1–3**.

The optical spectra of compounds **1–3** have been measured in the range 250–400 nm. The optical band gap for each of the films has been estimated from UV-vis spectrum using Tauc's equation (equation (S1)).¹³

$$(\alpha h\nu) = A(h\nu - E_g)^n \quad (\text{S1})$$

where, α , E_g , h and ν stand for absorption coefficient, band gap, Planck's constant and frequency of light. The exponent ' n ' is the electron transition processes dependent constant. ' A ' is a constant which is considered as 1 for ideal case. To calculate the direct optical band gap, the value of the exponent ' n ' in the above equation has been considered as $n = 1/2$.¹⁴ By extrapolating the linear region of the plot $(\alpha h\nu)^2$ vs. $h\nu$ (Fig. S16) to $\alpha = 0$ absorption, the values of direct optical band gap (E_g) of the compounds have been calculated as 3.71 eV, 3.74 eV, and 3.51 eV for compounds **1–3**, respectively.

Device fabrication

In this study, multiple metal-semiconductor (MS) junction thin film devices (**MSD1**, **MSD2** and **MSD3** with compounds **1**, **2** and **3** respectively) were fabricated in ITO/compound/Al sandwich structure to perform the electrical study. In this regard, well dispersion of the synthesized compounds (**1–3**) were made in *N,N*-dimethyl formamide (DMF) by mixing and sonicated the right proportion (25 mg/ml) of compounds in separate vials. This newly prepared stable dispersion of compounds were deposited on the top of the ITO coated glass substrate by spun firstly at 500 rpm for 4 min and thereafter at 800 rpm for 6 min with the help of SCU 2700 spin

coating unit. Afterward, all the as-deposited thin films were dried in a vacuum oven (at a base pressure of 5×10^{-3} Torr) at 90 °C for several minutes to evaporate the solvent part fully. The thicknesses of the developed films were measured by surface profiler as $\sim 1 \mu\text{m}$ (Fig. S17).

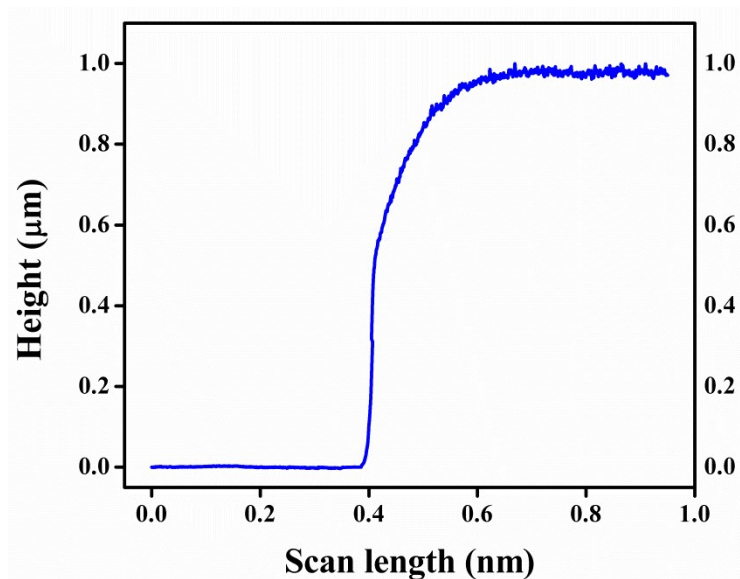
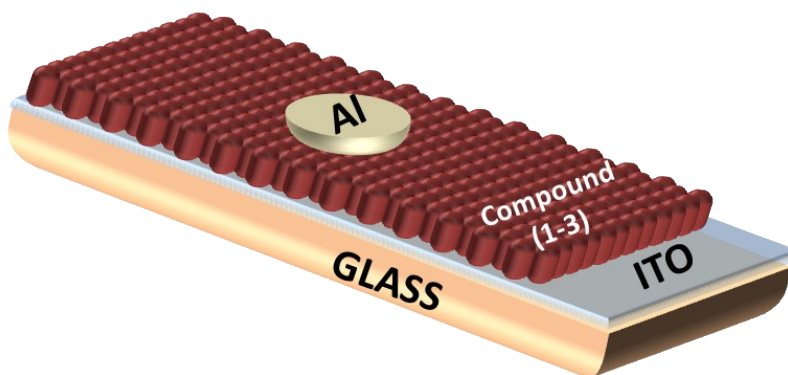


Fig. S17 Profilometer data for the measurement of film thickness.

The aluminium electrodes were deposited under base pressure (10^{-6} Torr) by maintaining the effective area as $7.065 \times 10^{-2} \text{ cm}^{-2}$ with shadow mask in the Vacuum Coating Unit 12A4D of HINDHIVAC. We have provided below the schematic diagram (Scheme S2) of our proposed fabricated synthesized compounds (1–3) based MS Schottky diode along with the optical image (Fig. S18) of the device showing the ITO substrate, film and electrodes.



Scheme S2. Schematic diagram of our proposed fabricated synthesized compounds (1–3) based MS Schottky diode.

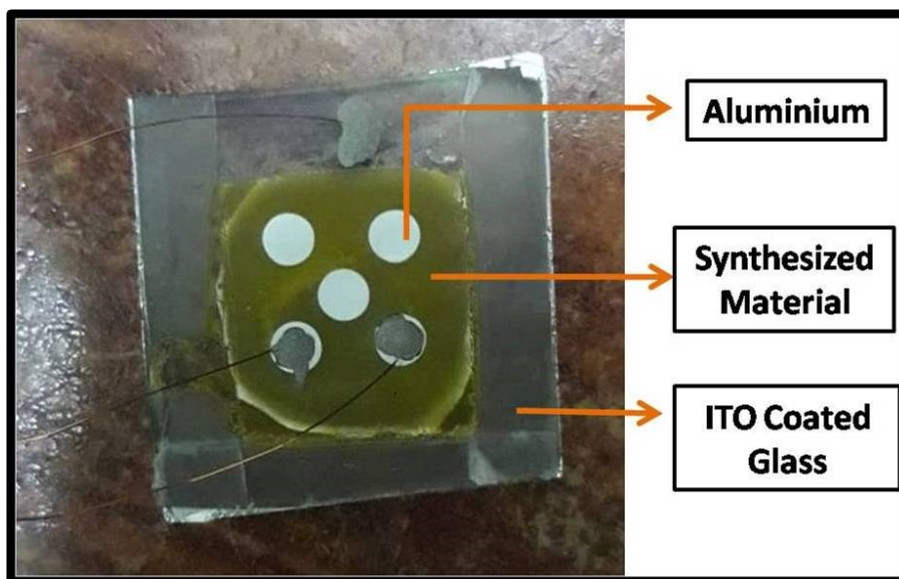


Fig. S18 Optical image of our fabricated synthesized compounds (1–3) based MS Schottky diode.

The potential probe is most commonly employed method for measuring the resistivity of samples with low resistance value. Potential drop across two probes is measured and the gap between them (D) is taken as the sample length, L . If the probes are not point contacts, true value of probe distance is gap between the centers and not the shortest distance between them. Two Probe technique is suitable for measuring resistivity of high resistivity samples, e.g., polymer films/sheets. Fig. S19 displays schematic demonstration of the experimental procedure. The resistivity, ρ , is calculated from the voltage drop (V) and current (I) as:

$$\rho = \frac{V.A}{I.L} \quad (S2)$$

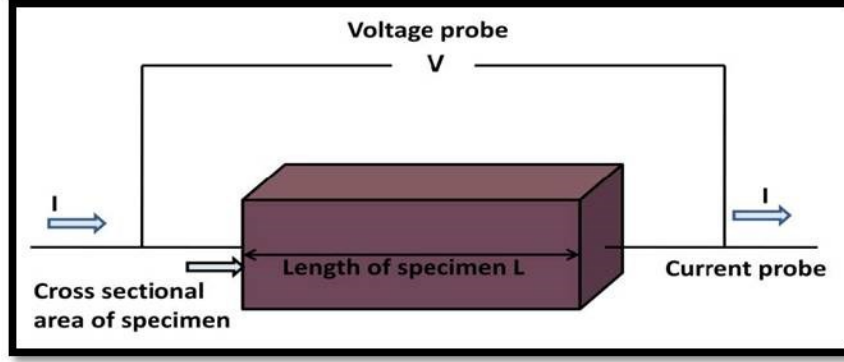


Fig. S19 Measuring electrical resistivity by two probe method.

For electrical characterization of the devices, the current-voltage ($I-V$) characteristic was measured under both dark and AM 1.5G radiation condition and recorded with the help of a Keithley 2635B Sourcemeter by two-probe technique. All the preparations and measurements were performed at room temperature and under ambient conditions.

Electrical property analysis

The $I-V$ characteristic of the synthesized BD SC based Schottky barrier diode (SBD) has been further analyzed by thermionic emission theory. Cheung's method has also been employed to extract important diode parameters.¹⁵ In this regard; the obtained $I-V$ curve has been analyzed quantitatively by considering the following standard equations:^{15,16}

$$I = I_0 \exp\left(\frac{qV}{\eta KT}\right) \left[1 - \exp\left(\frac{-qV}{\eta KT}\right)\right] \quad (\text{S3})$$

$$I_0 = AA^* T^2 \exp\left(\frac{-q\phi_B}{KT}\right) \quad (\text{S4})$$

where I_0 , k , T , V , A , η and A^* stands for saturation current, electronic charge, Boltzmann constant, temperature in Kelvin, forward bias voltage, effective diode area, ideality factor and effective Richardson constant, respectively. The effective Richardson constant was considered as $32 \text{ AK}^{-2} \text{ cm}^{-2}$ for the fabricated devices.

The series resistance, ideality factor and barrier potential height was also determined by using equations (S5) to (S7), which was extracted from Cheung's idea,^{15,16}

$$\frac{dV}{d(\ln I)} = \left(\frac{\eta KT}{q} \right) + IR_S \quad (S5)$$

$$H(I) = V - \left(\frac{\eta KT}{q} \right) \ln \left(\frac{I}{AA * T^2} \right) \quad (S6)$$

$$H(I) = IR_S + \eta \phi_B \quad (S7)$$

The deviation from the ideal value of 1 can be attributed to the presence at the junction of Schottky inhomogeneities, interface defect states and/or series resistance.^{17,18} On the other side, better homogeneity for the Schottky barrier at the MS interface and the recombination of less charge carriers upon light irradiation would explain the lower values of η for our devices.¹⁵ This fact indicates that our devices possess lesser recombination of carriers at the interface, i.e., a improved barrier homogeneity, with light irradiation.

The effective carrier mobility (μ_{eff}) can be determined employing the Mott-Gurney equation (equation (S8)) in the SCLC model with the high voltage data of the I vs. V^2 plot (Fig. 9):^{15,16,19}

$$I = \frac{9\mu_{eff}\epsilon_0\epsilon_r A (V^2)}{8 \left(\frac{d^3}{d^3} \right)} \quad (S8)$$

where, I , μ_{eff} , ϵ_r , and ϵ_0 are the current, the effective mobility, the relative dielectric constant and the free space permittivity of the material, respectively.

The dielectric constant of the material (ϵ_r) can be calculated from the saturation region of the capacitance vs. frequency curve at higher frequency (Fig. 10) with the equation given below:¹⁵

$$\epsilon_r = \frac{1}{\epsilon_0} \cdot \frac{C d}{A} \quad (S9)$$

where, C , d , and A are the capacitance at saturation, the thickness of the film ($\sim 1 \mu\text{m}$) and the device area, respectively. With this formula, we obtain ϵ_r values as 6.11×10^{-2} , 5.53×10^{-2} and 6.69×10^{-2} for compounds **1**, **2** and **3** respectively.

The study of the charge transport behavior through the junction, we have evaluated the value of transit time (τ) and diffusion length (L_D). The value of τ can be determined (using equation (S10)) from the slope of the I vs. V plot (Fig. 5) in the SCLC region (region II).¹⁵

$$\tau = \frac{9\epsilon_0\epsilon_r A (V)}{8d (I)} \quad (\text{S10})$$

$$\mu_{eff} = \frac{qD}{kT} \quad (\text{S11})$$

$$L_D = \sqrt{2D\tau} \quad (\text{S12})$$

where, D stands for diffusion coefficient that can be determined using Einstein-Smoluchowski equation (equation (S11)).¹⁵

Table S3 Comparison Table of Diode Parameters with Other Reported Data

Sample Name /Formula	Electrical Conductivity (S m ⁻¹)	Series Resistance (R_S) (Ohm)	Life Time (Sec)	Diffusion Length (L_D) (m)	Reference
Zn(OPE-C ₁₂)·2H ₂ O	9.6×10^{-6}	330	0.11×10^{-6}	198×10^{-9}	ref. 15
Oxalic Acid-Monoethanolamine Gel	4.42×10^{-4}	570	4.57×10^{-4}	1.22×10^{-7}	ref. 16
copper(II)-malonate 2-amino-4-methylpyridine	1.53×10^{-3}	676	11.11×10^{-5}	1.21×10^{-7}	ref. 17
copper(II)-malonate 2-aminopyrimidine	0.88×10^{-3}	715	8.36×10^{-5}	1.15×10^{-7}	ref. 17
[Zn(adc)(4-nvp) ₂ (H ₂ O) ₂]	9.29×10^{-4}	402	1.03×10^{-3}	7.83×10^{-8}	ref. 18
Terbium(III)- metallogel (Tb-OX)	3.54×10^{-5}	9560	2.42×10^{-9}	1.73×10^{-7}	ref. 19
Compound 3	19.38×10^{-4}	280.51	5.16×10^{-6}	4.69×10^{-8}	This work

Compound 2	16.54×10^{-4}	388.93	6.69×10^{-6}	3.86×10^{-8}	This work
Compound 1	15.47×10^{-4}	456.27	6.36×10^{-6}	4.38×10^{-8}	This work

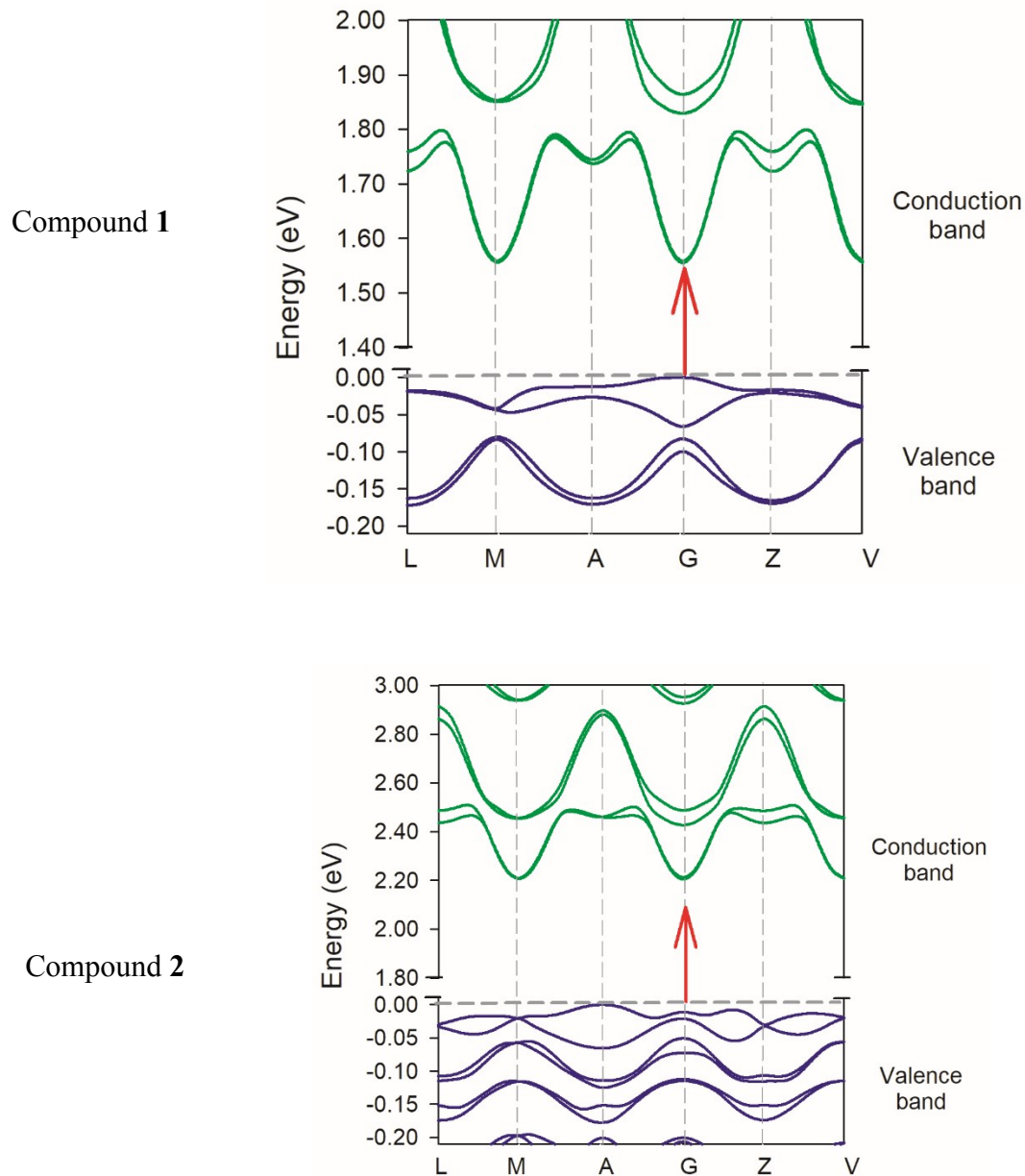


Fig. S20 Electronic band structures of the ground state of compounds **1** and **2**. Points of high symmetry in the first Brillouin zone are labeled as follows: L = (-0.5, 0, 0.5); M = (-0.5, 0.5, 0.5); A = (-0.5, 0, 0); G = (0, 0, 0); Z = (0, -0.5, 0.5); V = (0, -0.5, 0.5).

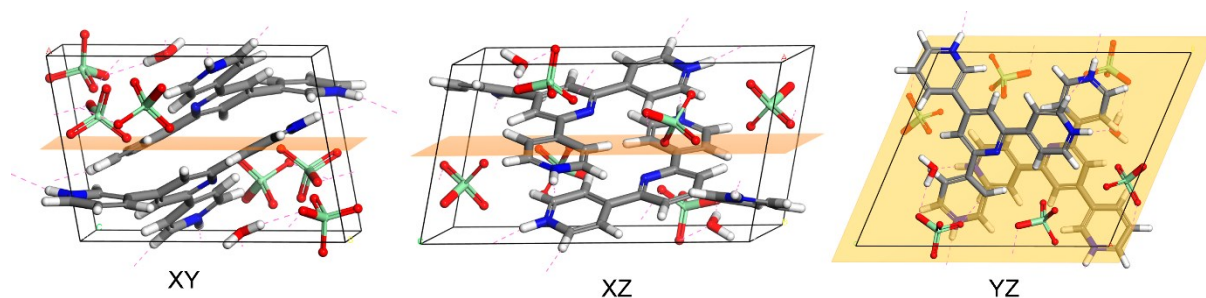


Fig. S21 The three-dimensional crystal faces of compound **3**. The (100) miller plane (orange plane) shows the orientation of ϵ_{xx} component of dielectric constant. Colour code: carbon (grey), hydrogen (white), nitrogen (blue), chlorine (green), oxygen (red).

References

1. S. J. Clark, M. D. Segall, C. J. Pickard, P. J. Hasnip, M. I. J. Probert, K. Refson and M. C. Payne, *Z. Kristallogr.*, **2005**, *220*, 567–570.
2. J. P. Perdew, K. Burke and M. Ernzerhof, *Phys. Rev. Lett.*, **1996**, *77*, 3865–3868.
3. J. P. Perdew, J. A. Chevary, S. H. Vosko, K. A. Jackson, M. R. Pederson, D. J. Singh and C. Fiolhais, *Phys. Rev. B.*, **1992**, *46*, 6671–6687.
4. D. Vanderbilt, *Phys. Rev. B*, **1990**, *41*, 7892–7895.
5. D. D. Koelling and B. N. Harmon, *J. Phys. C: Solid State Phys.*, **1977**, *10*, 3107–3114.
6. A. Tkatchenko and M. Scheffler, *Phys. Rev. Lett.*, **2009**, *102*, 073005.
7. Robb, J. R. Cheeseman, G. Scalmani, V. Barone, G. A. Petersson, H. Nakatsuji, X. Li, M. Caricato, A. Marenich, J. Bloino, B. G. Janesko, R. Gomperts, B. Mennucci, H. P. Hratchian, J. V. Ortiz, A. F. Izmaylov, J. L. Sonnenberg, D. Williams-Young, F. Ding, F. Lipparini, F. Egidi, J. Goings, B. Peng, A. Petrone, T. Henderson, D. Ranasinghe, V. G. Zakrzewski, J. Gao, N. Rega, G. Zheng, W. Liang, M. Hada, M. Ehara, K. Toyota, R. Fukuda, J. Hasegawa, M. Ishida, T. Nakajima, Y. Honda, O. Kitao, H. Nakai, T. Vreven, K. Throssell, J. A. Montgomery, Jr., J. E. Peralta, F. Ogliaro, M. Bearpark, J. J. Heyd, E. Brothers, K. N. Kudin, V. N. Staroverov, T. Keith, R. Kobayashi, J. Normand, K. Raghavachari, A. Rendell, J. C. Burant, S. S. Iyengar, J. Tomasi, M. Cossi, J. M. Millam, M. Klene, C. Adamo, R. Cammi, J. W. Ochterski, R. L. Martin, K. Morokuma, O. Farkas,

- J. B. Foresman, D. J. Fox, Gaussian 16 (Revision A.03), Gaussian Inc., Wallingford CT, 2016.
8. S. Grimme, J. Antony, S. Ehrlich and H. Krieg, *J. Chem. Phys.*, 2010, **132**, 154104.
 9. R. F. W. Bader, *Chem. Rev.*, 1991, **91**, 893–928
 10. J. Contreras-Garcia, E. Johnson, S. Keinan, R. Chaudret, J.-P. Piquemal, D. Beratan and W. Yang, *J. Chem. Theor. Comp.*, 2011, **7**, 625–632.
 11. T. A. Keith, AIMAll (Version 19.02.13), TK Gristmill Software, Overland Park KS, USA, 2019 (aim.tkgristmill.com).
 12. A. Bondi, *J. Phys. Chem.*, 1964, **68**, 441–451.
 13. A. Dey, S. Middya, R. Jana, M. Das, J. Datta, A. Layek and P. P. Ray, *J. Mater. Sci.: Mater. Electron.*, **2016**, *27*, 6325–6335.
 14. E. H. Rhoderick, *Metal Semiconductors Contacts*, Oxford University, Press, Oxford, **1978**.
 15. S. K. Cheung and N. W. Cheung, *Appl. Phys. Lett.*, **1986**, *49*, 85–87.
 16. A. Dey, A. Layek, A. Roychowdhury, M. Das, J. Datta, S. Middya, D. Das and P. P. Ray, *RSC Adv.*, **2015**, *5*, 36560–36567.
 17. R. K. Gupta and F. Yakuphanoglu, *Solar Energy.*, **2012**, *86*, 1539–1545.
 18. X. Miao, S. Tongay, M. K. Petterson, K. Berke, A. G. Rinzler, B. R. Appleton and A. F. Hebard, *Nano Lett.*, **2012**, *12*, 2745–2750.
 19. P. W. M. Blom, M. J. M. de Jong and M. G. van Munster, *Phys. Rev. B*, **1997**, *55*, R656–R659.